Materials Research. 2017; 20(2): 407-412
DOI: http://dx.doi.org/10.1590/1980-5373-MR-2016-0561

Effect of Cupric Salts ($Cu(NO_3)_2$, $CuSO_4$, $Cu(CH_3COO)_2$) on $Cu_2(OH)PO_4$ Morphology for Photocatalytic Degradation of 2,4-dichlorophenol under Near-infrared light irradiation

*Chao Hu[a], Pei Li[a], Wei Zhang[a], Yanhao Che[a], Yaxin Sun[a], Fangli Chi[a], Songlin Ran[a], Xianguo Liu[a], Yaohui Lv[a]**

[a] *School of Materials Science and Engineering, Anhui Key Laboratory of Metal Materials and Processing, Anhui University of Technology, Anhui, Maanshan, 243002, P. R. China*

Received: July 27, 2016; Revised: December 22, 2016; Accepted: December 27, 2016

$Cu_2(OH)PO_4$ microstructures were synthesized by the hydrothermal method using three different types cupric salts ($Cu(NO_3)_2$, $CuSO_4$, $Cu(CH_3COO)_2$) as raw materials. The X-ray diffraction (XRD), scanning electron microscopy (SEM) and UV-visible-NIR absorption spectra were used to characterize the as-obtained products. The different anions (SO_4^{2-}, CH_3COO^-, NO_3^-) have different shapes and polarities, which can generate different interactions in reaction bath, induced the difference of structure and morphology of the prepared $Cu_2(OH)PO_4$. The $Cu_2(OH)PO_4$ microstructures prepared form $Cu(NO_3)_2 \cdot 3H_2O$ showed the best photocatalytic activity induced by near-infrared light to degrade 2,4-dichlorophenol (2,4-DCP) solution. Our work suggests that the active morphological surfaces as well as different coordination environments for the metal ions has an important influence on the photocatalytic performance of $Cu_2(OH)PO_4$ microstructure.

Keywords: *$Cu_2(OH)PO_4$; Morphology; Near-infrared light; Photocatalytic performance*

1. Introduction

In the past decades, semiconductor has attracted significant attention owing to their applicability in solar energy conversion and environmental protection[1-3]. However, due to the wide band gaps of the semiconductor photocatalysts, a large part of solar energy cannot be utilized, especially the near-infrared (NIR) region, which accounts for about 44% of the incoming solar energy[4]. Over the past 30 years, the search for near-infrared light photocatalysts has focused mainly on upconversion luminescence of rare earth materials[5-7]. The rare earth materials can transfer near-infrared light to UV or visible light active photocatalysts to generate the strongly oxidative holes and reductive electrons[8]. Although this work demonstrated the possibility of using NIR light for photocatalysis, a 980-nm laser had to be used for an overall low conversion, thus exemplifying the limited applicability of this strategy for solar light photocatalysis[9]. Besides up-conversion materials, only a few of near-infrared photocatalysts have been found, such as Bi_2WO_6[9], carbon quantum dots[10], WS_2[1], $Cu_2(OH)PO_4$[11]. It is still a challenging task to further expand the light absorption range of photocatalysts and develop IR-driven photocatalysts to utilize more solar energy.

Among this near-infrared photocatalyst, copper hydroxyphosphate ($Cu_2(OH)PO_4$) has attracted special attention due to its unique near-infrared photocatalytic properties[12]. It has an orthorhombic crystal structure with cell parameters of a=8.062, b=8.384, and c=5.881Å and consists of a PO_4 tetrahedron, a Cu(1)O_6 octahedron, a Cu(2)O_5 trigonal bipyramid, and an OH group between the two Cu species, in which oxygen atoms are shared with each other (shown in Figure S1)[13]. $Cu_2(OH)PO_4$ can be synthesized by several methods either the precipitation or hydrothermal methods because it is a simple method and a low-cost technique. Copper nitrate ($Cu(NO_3)_2 \cdot 3H_2O$) is the most popular agent to form $Cu_2(OH)PO_4$ powders[14-16], however, some different copper sources such as $Cu(CH_3COO)_2$ or $CuSO_4$ have been reported for use[17-19]. However, the effect of different types of copper salts on the morphology of $Cu_2(OH)PO_4$ has not been reported. It appears that the type of copper salts can control the morphology of $Cu_2(OH)PO_4$ and then has an effect on its properties, including its photocatalytic activity.

In this work, we report the effect of cupric salts ($Cu(NO_3)_2$, $CuSO_4$, $Cu(CH_3COO)_2$) on the structure, morphology and photocatalytic activity of $Cu_2(OH)PO_4$ prepared through hydrothermal method. The crystal structures and optical properties of the prepared powders were characterized using X-ray diffraction (XRD) and UV-Vis-NIR diffuse reflectance spectroscopy. Lastly, the photocatalytic properties for the degradation of 2,4-dichlorophenol (2,4-DCP) solution under near-infrared light irradiation were also evaluated.

2. Experimental section

2.1. Synthesis

$Cu_2(OH)PO_4$ microcrystals were prepared by a hydrothermal method. In a typical procedure, 20 mmol of $Cu(NO_3)_2 \cdot 3H_2O$ and 10 mmol $Na_2HPO_4 \cdot 12H_2O$ were mixed into deionized

* e-mail: yaohui2015@163.com

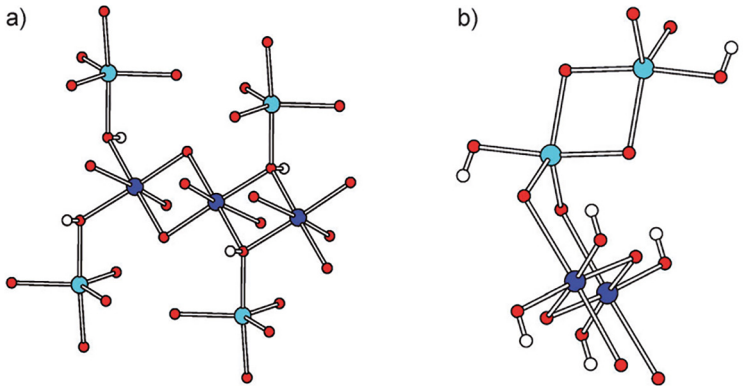

Figure S1: Views showing the corner-sharing between $CuO_4(OH)_2$ octahedra and $CuO_4(OH)$ trigonal bipyramids in $Cu_2(OH)PO_4$. For $CuO_4(OH)_2$ octahedra, O red, H white, and Cu blue; for $CuO_4(OH)$ trigonal bipyramids, Cu cyan. (a) Corner-sharing through OH groups; (b) Corner-sharing through O atoms. All O atoms, except for those in the OH groups, are corner-shared with PO_4 tetrahedra[1].

water (ca. 40 mL) under constant stirring for 1h, and the pH of the suspension was adjusted to 7 using 1 mol/L $NH_3 \cdot H_2O$ or 1 mol/L HNO_3. The bluish slurry mixture was then transferred to a Teflon-lined stainless steel autoclave, which was filled with deionized water up to 80% of its capacity (50 mL). The autoclave was heated to 120 °C in 30 min and maintained at this temperature for 6 h under autogenous pressure and static conditions. After reaction, the suspension was cooled to room temperature naturally. The deep green crystals were collected and washed several times with distilled water and absolute ethanol to remove impurities. The final products were dried at 50 °C (more than 10 h) for further characterizations. $Cu_2(OH)PO_4$ prepared from $Cu(NO_3)_2 \cdot 3H_2O$, $CuSO_4 \cdot 5H_2O$ and $Cu(CH_3COO)_2 \cdot H_2O$ have been labeled C-0, C-1 and C-2,respectively.

2.2. Characterization

The structural identification and morphology of the $Cu_2(OH)PO_4$ powders was carried out using an X-ray diffractometer (XRD, D8 Advance, Bruker AXS) with Cu Kα radiation at a wavelength of 0.15406 nm and a field emission scanning electron microscope (FESEM, S-4800, Hitachi), respectively. UV-Vis-NIR diffuse reflectance spectra (DRS) of the samples were recorded on a UV-Vis-NIR spectrophotometer (Cary 5000, Varian) with an integrating sphere attachment within the range of 200-1400 nm and with $BaSO_4$ as the reference standard.

2.3. Photocatalytic Study

The photocatalytic properties of the as-obtained samples were evaluated by measuring the degradation of 2,4-DCP under NIR light irradiation. A 350-W infrared lamp as the near-infrared light sources where the $\lambda > 760$ nm was filtered out during near-infrared light photocatalysis. Typically, 50 mg of sample powder was dispersed in 50 mL of 2,4-DCP aqueous solution (c=20 mg L^{-1}). The scheme diagram of the experimental photocatalytic apparatus was shown in Figure S2. Prior to photoirradiation, the suspensions were magnetically stirred in the dark for 30 min (widespread adoption of time) to attain the adsorption/desorption equilibrium between the dye and the surface of the catalyst under ambient conditions. At varied irradiation time intervals, 3 mL suspension was collected, centrifuged and analyzed by UV-Vis spectroscopic measures (Hitachi UV-3100). The 285 nm wavelength was used to quantify the degradation of 2.4-dichlorophenol.

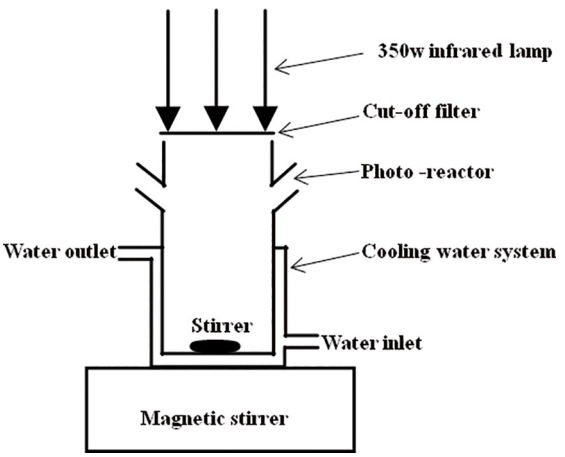

Figure S2: The picture of scheme of our experimental photocatalytic apparatus.

3. Results and Discussion

The X-ray diffraction (XRD) patterns of $Cu_2(OH)PO_4$ prepared with three different types of cupric salts are shown in Figure 1, all peaks can be clearly indexed as the

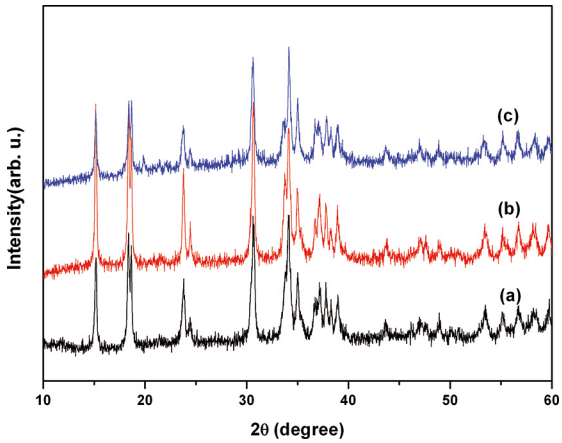

Figure 1: X-ray diffraction patterns of $Cu_2(OH)PO_4$ prepared from three different types of cupric salts as raw materials (a) $Cu(NO_3)_2$•$3H_2O$; (b) $CuSO_4$•$5H_2O$; (c) $Cu(CH_3COO)_2$•H_2O

pure orthorhombic phase as all diffraction peaks of these samples are well matched with JCPDS card number 36-0404. The ration difference between diffraction peaks of different samples may be induced by the different exposed crystal faces. The amount of different exposed crystal faces can induce the difference of intensity of diffraction peak. No diffraction peaks for other phases or materials (such as pseudomalachite $[Cu_5(OH)_4(PO_4)_2]$) or copper phosphate hydrate $[Cu_3(PO_4)_2$•$3H_2O]$ are observed in XRD patterns, indicating a high purity and crystallinity of the final products. The average particle diameter is 36.1 nm, 37.5 nm and 38.3 nm for C-0, C-1 and C-2, respectively. The diameter was calculated by using the Scherrer equation, $D=k\lambda/\beta\cos\theta$, where k is a dimensionless shape factor, with a value close to unity (~0.9); λ is the X-ray wavelength (0.15406 nm); β is the line broadening at half the maximum intensity (FWHM), after subtracting the instrumental line broadening (obtained by deducting the background applying the Jade 6.0 software in our experiment); θ is the Bragg angle, which is obtained from the stronger peak in our experiment.

Figure 2 (a-d) show the FESEM images for $Cu_2(OH)PO_4$ with three different cupric salts, respectively. It is clear that the different anions have an obvious effect on the surface morphology of the obtained product. A typical SEM image of $Cu_2(OH)PO_4$ microstructures with rugby-like morphology is obtained from the precursor of $Cu(NO_3)_2 \cdot 3H_2O$ and $Na_2HPO_4 \cdot 12H_2O$ as shown in Figure 2a. The results show that rugby-like $Cu_2(OH)PO_4$ microstructures was assembled with isotropic and highly aggregated nanoparticles. The size of the nanoparticles was about 100 nm. For the study of sulfate anion effect on the morphology of $Cu_2(OH)PO_4$ microstructures, an equimolar solution was prepared by dissolving the $CuSO_4 \cdot 5H_2O$ and $Na_2HPO_4 \cdot 12H_2O$. In this case, the $Cu_2(OH)PO_4$ microstructures with balsam pear-like morphology is obtained as shown in Figure 2b. The balsam pear-like $Cu_2(OH)PO_4$ microstructures was assembled with highly isotropic and aggregated nanoparticles with rod-like nanocrystals of 100 nm length and 20 nm width. In addition, the rod-like nanocrystals has the smooth surface. For the study of acetate anion effect on the morphology of $Cu_2(OH)PO_4$ microstructures a spherical-like morphology based on interconnected network of nanoplates were obtained as shown in Figure 2(c-d). Similar reactions were participated in the synthesis of various morphologies of $Cu_2(OH)PO_4$ microstructures irrespective source of Cu^{2+} ion was different. When SO_4^{2-}, CH_3COO^-, or NO_3^- is added to the reaction bath, different anions can generate the following problem: (1) different anions (SO_4^{2-}, CH_3COO^-, or NO_3^-, etc.) have different shapes and polarities, which can generate different interactions in reaction bath; (2) different anions of cupric salts can generate different deposition environments and form different solution effects or bonds between reaction and non-reaction molecules in solution, which affect diffusion and adsorption of complex precursor ions significantly.

To evaluate the optical absorption properties of $Cu_2(OH)PO_4$ with various morphologies, the UV-Vis-NIR absorption spectra were investigated (Figure 3). The results show that the $Cu_2(OH)PO_4$ microstructures prepared with $Cu(NO_3)_2 \cdot 3H_2O$ as raw material (H-0) have very broad absorption band and higher intensity (Figure 3a). The absorption peak of the $Cu_2(OH)PO_4$ microstructures prepared with $Cu(CH_3COO)_2$ as raw material (H-2) is located at 520 nm (Figure 3c). It is noteworthy that there is no any absorption in the near-infrared region. Compared to the sample H-2, the $Cu_2(OH)PO_4$ microstructures prepared with $CuSO_4 \cdot 5H_2O$ as raw material (H-1) have broader absorption band and higher intensity (Figure 3b). The absorption intensity obtained in the presence of the three copper salts is affected by the anion in the following order: $NO_3^- > SO_4^{2-} > CH_3COO^-$. Remarkable absorption enhancement in near-infrared light region is beneficial for improving photocatalytic activity in this irradiation region.

Figure 4 shows the variations of the photocatalytic degradation of 2,4-DCP as a function of irradiation times, where C represents concentration of 2,4-DCP at the irradiation time (t) and C_0 is the concentration of the 2,4-DCP before irradiation. It is evident that without using any photocatalyst, 15% of the 2,4-DCP molecules were degraded after the light irradiation for 6h (Figure 4a). The H-0 sample possesses enhanced near-infrared photocatalytic activities compared with H-1 sample. The 2,4-DCP —degradation degree for $Cu_2(OH)PO_4$ microstructures (H-1) and $Cu_2(OH)PO_4$ microstructures (H-0) under 6 h near-infrared light irradiation is 35% and 70%, respectively(Figure 4c and Figure 4d). Figure S3 shows temporal evolution of the spectral changes during photocatalytic degradation of RhB solution over $Cu_2(OH)PO_4$ (H-1) under NIR-light irradiation for various time periods. From Figure S3, it could be seen that with increase of irradiation time in aqueous suspension, the intensity of the absorption peak decreased, which indicated that the

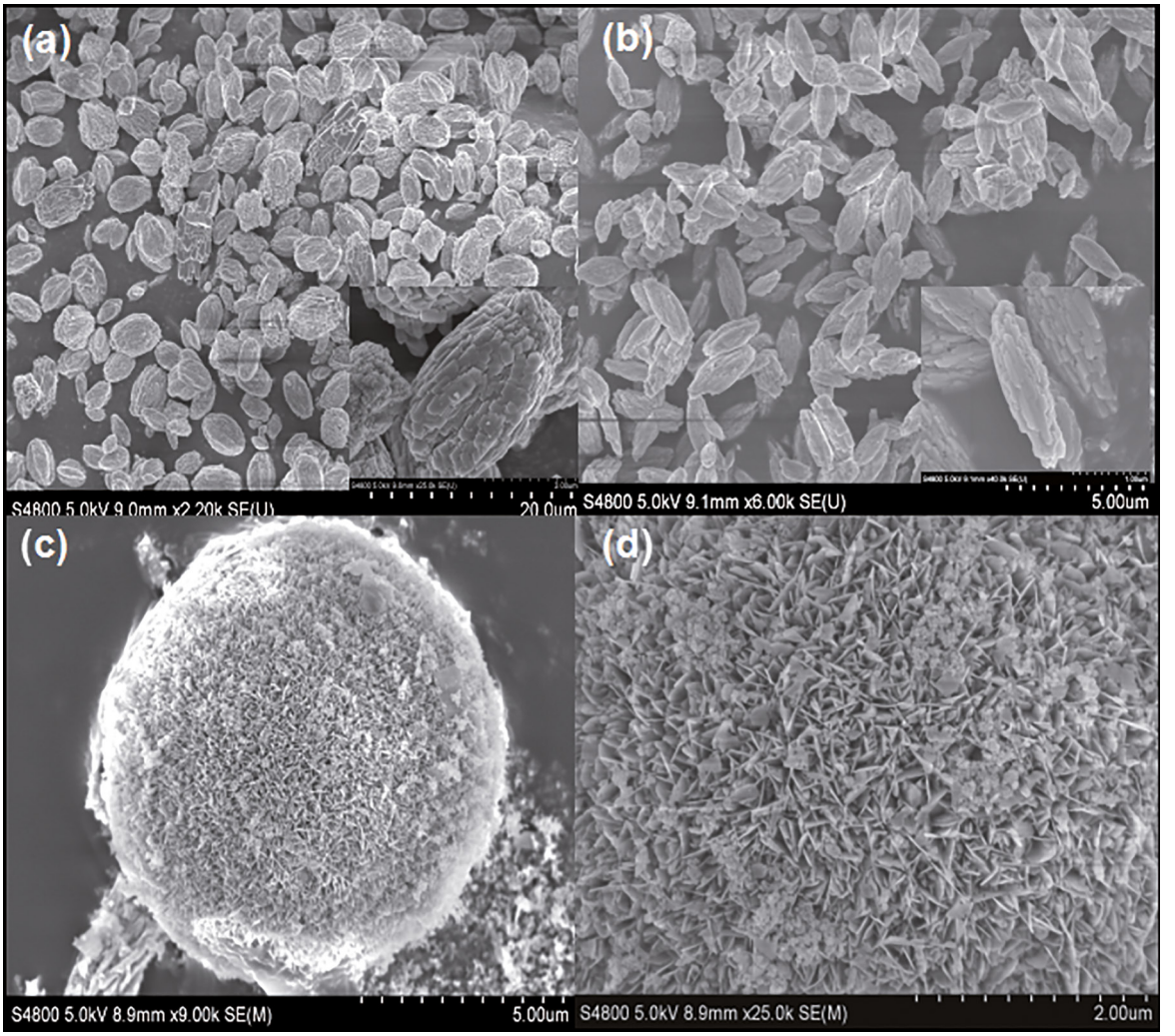

Figure 2: Scanning electron microscope images of $Cu_2(OH)PO_4$ prepared from three different types of cupric salts as raw materials (a) $Cu(NO_3)_2$•$3H_2O$; (b) $CuSO_4$•$5H_2O$; (c) (d) $Cu(CH_3COO)_2$•H_2O

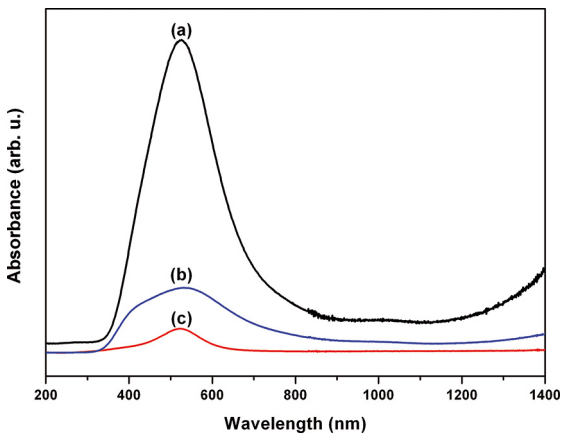

Figure 3: UV-Vis-NIR absorption spectra of $Cu_2(OH)PO_4$ prepared from three different types of cupric salts as raw materials (a) $Cu(NO_3)_2$•$3H_2O$; (b) $CuSO_4$•$5H_2O$; (c) $Cu(CH_3COO)_2$•H_2O

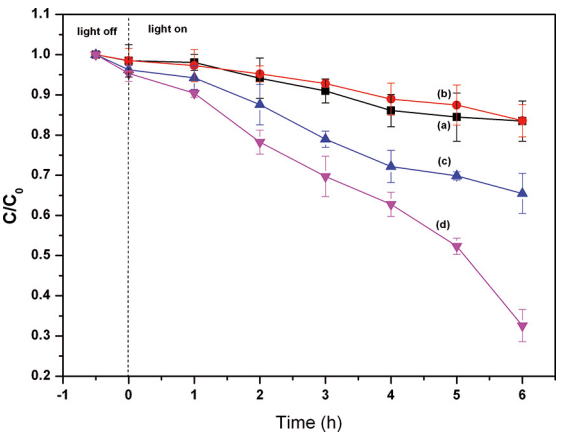

Figure 4: Photocatalytic degradation of 2,4-DCP by $Cu_2(OH)PO_4$ prepared from three different types of cupric salts as raw materials under near-infrared light irradiation (a) 2,4-DCP self-decomposition; (b) $Cu(CH_3COO)_2$•H_2O; (c) $CuSO_4$•$5H_2O$; (d) $Cu(NO_3)_2$•$3H_2O$

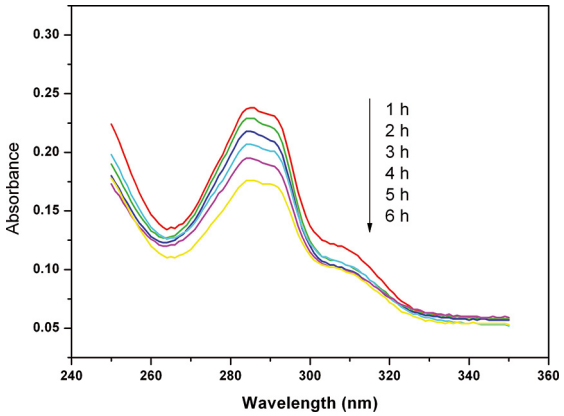

Figure S3: UV-vis spectral changes of 2,4-dichlorophenol in aqueous $Cu_2(OH)PO_4$ (H-1) sample as a function of irradiation time.

$Cu_2(OH)PO_4$ (H-1) exhibited good photocatalytic activity. In contrast, the $Cu_2(OH)PO_4$ microstructures (H-2) have no near-infrared photodegradation ability to 2,4-DCP (Figure 4b). Therefore, it was observed that rugby-like $Cu_2(OH)PO_4$ exhibited significantly higher photocatalytic activity for the photodegradation of 2,4-DCP than that of balsam pear-like and spherical-like $Cu_2(OH)PO_4$ microstructures. The mechanism of photocatalytic reaction for $Cu_2(OH)PO_4$ under NIR light irradiation is not clear. Huang BB et al [11] examined the electronic band structure of $Cu_2(OH)PO_4$ by performing density functional theory (DFT) calculations, and pointed out that the photogenerated electrons from the $CuO_4(OH)$ trigonal bipyramids that reach the upper three unoccupied bands are easily transferred to the $CuO_4(OH)_2$ octahedra. Our experimental results indicate the active morphological surfaces of $Cu_2(OH)PO_4$ microstructures can determine the photocatalytic activity. As is well-known, the surface area has an important influence on the photocatalytic activity. Especially, the photocatalytic activity of nanomaterial is better than the photocatalytic performance of the micromaterial. In this experiment, due to the larger size of particle, thus, the surface area of the sample has the little influence on the observed photocatalytic performance. In addition, the standard deviations of the degradation efficiency were always below 6%, indicating the good reproducibility of the photocatalytic evaluation.

4. Conclusions

The type of cupric salts used as different raw materials can affect the morphology, particle size and photocatalytic activity of the obtained $Cu_2(OH)PO_4$ powder. Using $Cu(NO_3)_2 \cdot 3H_2O$ as raw material, rugby-like $Cu_2(OH)PO_4$ microstructures was obtained and exhibited significantly higher photocatalytic activity for the photodegradation of 2,4-DCP. However, when the raw materials are $CuSO_4 \cdot 5H_2O$ and $Cu(CH_3COO)_2 \cdot H_2O$, the products showed balsam pear-like and spherical-like morphology, respectively. In addition, the products obtained from $CuSO_4 \cdot 5H_2O$ and $Cu(CH_3COO)_2 \cdot H_2O$ as raw materials has the poor near-infrared light photocatalytic performance. Our work suggest that the active morphological surfaces of $Cu_2(OH)PO_4$ microstructures have an important influence on the photocatalytic activity.

5. Acknowledgements

This research was financially supported by the Natural Science Foundation of AnHui Provincial Education Department (KJ2015A085, KJ2016A102) and Graduate Student Innovation Fund of Anhui University of Technology.

6. References

1. Sang Y, Zhao Z, Zhao M, Hao P, Leng Y, Liu H. From UV to Near-Infrared, WS_2 Nanosheet: A Novel Photocatalyst for Full Solar Light Spectrum Photodegradation. *Advanced Materials*. 2015;27(2):363-369. DOI: 10.1002/adma.201403264

2. Lv Y, Liu H, Zhang W, Ran S, Chi F, Yang B, et al. Room-temperature synthesis and high visible-light-induced photocatalytic activity of AgI/BiOI composites. *Journal of Environmental Chemical Engineering*. 2013;1(3):526-533. DOI: 10.1016/j.jece.2013.06.019

3. Lv Y, Huang K, Zhang W, Yang B, Chi F, Ran S, et al. One step synthesis of $Ag/Ag_3PO_4/BiPO_4$ double-heterostructured nanocomposites with enhanced visible-light photocatalytic activity and stability. *Ceramics International*. 2014;40(6):8087-8092. DOI: 10.1016/j.ceramint.2013.12.162

4. Sang Y, Liu H, Umar A. Photocatalysis from UV/Vis to Near-Infrared Light: Towards Full Solar-Light Spectrum Activity. *ChemCatChem*. 2015;7(4):559-573. DOI: 10.1002/cctc.201402812

5. Ren L, Qi X, Liu Y, Huang Z, Wei X, Li J, et al. Upconversion-P25-graphene composite as an advanced sunlight driven photocatalytic hybrid material. *Journal of Materials Chemistry*. 2012;22(23):11765-11771. DOI: 10.1039/C2JM30457K

6. Li Z, Li C, Mei Y, Wang L, Du G, Xiong Y. Synthesis of rhombic hierarchical YF_3 nanocrystals and their use as upconversion photocatalysts after TiO_2 coating. *Nanoscale*. 2013;5(7):3030-3036. DOI: 10.1039/C3NR34018J

7. Huang S, Guo S, Wang Q, Zhu N, Lou Z, Li L, et al. CaF_2-Based Near-Infrared Photocatalyst Using the Multifunctional $CaTiO_3$ Precursors as the Calcium Source. *ACS Applied Materials & Interfaces*. 2015;7(36):20170-20178. DOI: 10.1021/acsami.5b05557

8. Wang Z, Liu Y, Huang B, Dai Y, Lou Z, Wang G, et al. Progress on extending the light absorption spectra of photocatalysts. *Physical Chemistry Chemical Physics*. 2014;16(7):2758-2774. DOI: 10.1039/C3CP53817F

9. Tian J, Sang Y, Yu G, Jiang H, Mu X, Liu H. A Bi_2WO_6-Based Hybrid Photocatalyst with Broad Spectrum Photocatalytic Properties under UV, Visible, and Near-Infrared Irradiation. *Advanced Materials*. 2013;25(36):5075-5080. DOI: 10.1002/adma.201302014

10. Li H, Liu R, Lian S, Liu Y, Huang H, Kang Z. Near-infrared light controlled photocatalytic activity of carbon quantum dots for highly selective oxidation reaction. *Nanoscale*. 2013;5(8):3289-3297. DOI: 10.1039/C3NR00092C

11. Wang G, Huang B, Ma X, Wang Z, Qin X, Zhang X, et al. $Cu_2(OH)PO_4$, a near-infrared-activated photocatalyst. *Angewandte Chemie (International ed. in English)*. 2013;52(18):4810-4813. DOI: 10.1002/anie.201301306

12. Li Z, Dai Y, Ma X, Zhu Y, Huang B. Tuning photocatalytic performance of the near-infrared-driven photocatalyst $Cu_2(OH)PO_4$ based on effective mass and dipole moment. *Physical Chemistry Chemical Physics*. 2014;16(7):3267-3273. DOI: 10.1039/C3CP53381F

13. Chen C, Zhou Y, Wang N, Cheng L, Ding H. $Cu_2(OH)PO_4$/g-C_3N_4 composite as an efficient visible light-activated photo-fenton photocatalyst. *RSC Advances*. 2015;5(116):95523-95531. DOI: 10.1039/C5RA15965B

14. Cho IS, Kim DW, Lee S, Kwak CH, Bae ST, Noh JH, et al. Synthesis of Cu_2PO_4OH Hierarchical Superstructures with Photocatalytic Activity in Visible Light. *Advanced Functional Materials*. 2008;18(15):2154-2162. DOI: 10.1002/adfm.200800167

15. Han J, Li H, Xu X, Yuan L, Wang N, Yu H. $Cu_2(OH)PO_4$ pretreated by composite surfactants for the micro-domino effect: A high-efficiency Fenton catalyst for the total oxidation of dyes. *Materials Letters*. 2016;166:71-74. DOI: 10.1016/j.matlet.2015.12.046

16. Kwak CH, Cho IS, Lee S, An JS, Hong KS. Hydrothermal Synthesis, Characterization and Photocatalytic Properties of Cu_2PO_4OH with Hierarchical Morphologies. *Journal of Nanoscience and Nanotechnology*. 2010;10(2):1185-1190. DOI: 10.1166/jnn.2010.1844

17. Xu Y, Wang C, Yang S. Uniform copper hydroxyphosphate microstructures with tunable size: Synthesis by a facile surfactant-free hydrothermal route and photocatalytic properties. *Materials Letters*. 2012;78:46-49. DOI: 10.1016/j.matlet.2012.03.054

18. Meng XJ, Sun JM, Yang M, Jiang D, Xiao FS. Catalytic Epoxidation of Styrene over Copper Hydroxyphosphate $Cu_2(OH)PO_4$. *Catalysis Letters*. 2001;71(3-4):241-244. DOI: 10.1023/A:1009051104167

19. Meng XJ, Sun ZH, Wang RW, Lin S, Sun JM, Yang M, et al. Catalytic Epoxidation of Styrene by Molecular Oxygen over a Novel Catalyst of Copper Hydroxyphosphate $Cu_2(OH)PO_4$. *Catalysis Letters*. 2001;76(1-2):105-109. DOI: 10.1023/A:1016755404975